Physics Letters B 838 (2023) 137651

Contents lists available at ScienceDirect

Physics Letters B

journal homepage: www.elsevier.com/locate/physletb

Correlating the CDF W-boson mass shift with the $b \to s\ell^+\ell^-$ anomalies

Xin-Qiang Li [a], Ze-Jun Xie [a], Ya-Dong Yang [a,b], Xing-Bo Yuan [a,*]

[a] Institute of Particle Physics and Key Laboratory of Quark and Lepton Physics (MOE), Central China Normal University, Wuhan, Hubei 430079, China
[b] Institute of Particle and Nuclear Physics, Henan Normal University, Xinxiang, Henan 453007, China

ARTICLE INFO

Article history:
Received 26 May 2022
Received in revised form 29 September 2022
Accepted 23 December 2022
Available online 5 January 2023
Editor: B. Grinstein

ABSTRACT

The recently updated measurement of the W-boson mass by the CDF collaboration exhibits a 7σ deviation from the SM expectation, which may imply a sign of new physics beyond the SM. The observed discrepancy could be explained by new fermions that carry the electroweak gauge charges and affect the vacuum polarization of gauge bosons. Notably, if the new fermions also have the same quantum numbers as of the SM quarks, they can mix with the latter and thus modify the penguin diagrams governing the $b \to s\ell^+\ell^-$ transitions. Therefore, the W-boson mass shift could be related to the $b \to s\ell^+\ell^-$ anomalies observed by the LHCb collaboration during the past few years. To investigate this possibility, we consider in this letter a model containing a vector-like top partner gauged under a new $U(1)'$ symmetry. It is found that the latest CDF m_W measurement and the $b \to s\ell^+\ell^-$ anomalies can be simultaneously accommodated at 2σ level.

1. Introduction

The Standard Model (SM) of particle physics has been remarkably successful in explaining most phenomena observed in experiments [1]. After the discovery of the Higgs boson [2,3], one important goal of the Large Hadron Collider (LHC) and its high-luminosity upgrade is the direct searches for new phenomena beyond the SM [4]. While the LHC has not yet discovered any direct evidence of new physics (NP) beyond the SM, several interesting deviations from the SM predictions have been emerging from the precision measurements, such as the anomalies observed in $b \to s\ell^+\ell^-$ processes [5–7].

In the field of precision measurements, the electroweak (EW) precision observables have played an important role in establishing the structure of the EW sector of the SM and can provide a sensitive probe of NP [8–10]. Recently, using the complete dataset collected by the CDF II detector at the Fermilab Tevatron, corresponding to 8.8 fb^{-1} of integrated luminosity, the CDF collaboration has reported an updated measurement of the W-boson mass [11]

$$m_W^{\rm CDF} = 80.4335 \pm 0.0064_{\rm stat} \pm 0.0069_{\rm syst}\ {\rm GeV}. \tag{1}$$

Interestingly, such a high precision measurement shows a 7σ deviation from the SM expectation obtained by a global EW fit, $m_W^{\rm SM} = 80.357 \pm 0.006$ GeV [1]. The latest CDF result also shows a significant shift compared to the average of the previous measurements from LEP, CDF, D0 and ATLAS, $m_W^{\rm PDG} = 80.379 \pm 0.012$ GeV [1], as well as the LHCb measurement, $m_W^{\rm LHCb} = 80.354 \pm 0.031$ GeV [12]. If confirmed by future measurements, the discrepancy could imply a sign of NP beyond the SM and has motivated numerous studies of the phenomenological implications of such a marvellous measurement (see, *e.g.*, refs. [13–39]).

The latest CDF W-boson mass shift could be induced by new fermions, which carry the EW gauge charges and contribute to the vacuum polarization of gauge bosons [40–45]. Notably, if the new fermions also have the same quantum numbers as of the SM quarks, they can mix with the latter and thus modify the γ- and Z-penguin diagrams that govern the flavour-changing neutral-current (FCNC) $b \to s$ transitions. Therefore, the observed discrepancy of the latest CDF m_W measurement could be related to the $b \to s\ell^+\ell^-$ anomalies observed by the LHCb collaboration [46–50]. To investigate this possibility, we consider in this letter the NP model introduced in ref. [51]. Specifically, the model is characterized by a vector-like top partner with an additional $U(1)'$ gauge symmetry, where the top quark and the top partner have the same quantum numbers under the SM gauge symmetry, while only the latter is charged under the $U(1)'$ symmetry. Similar models have been investigated, *e.g.*, in refs. [52–58].

* Corresponding author.
E-mail addresses: xqli@mail.ccnu.edu.cn (X.Q. Li), xiezejun@mails.ccnu.edu.cn (Z.J. Xie), yangyd@ccnu.edu.cn (Y.D. Yang), y@ccnu.edu.cn (X.B. Yuan).

https://doi.org/10.1016/j.physletb.2022.137651

This letter is organized as follows. In section 2, we introduce the NP model. In section 3, the top-partner contributions to the W-boson mass shift and the oblique parameters S, T and U are investigated. In section 4, we consider and compute the NP contributions to the $b \to s\ell^+\ell^-$ transitions. In section 5, we first derive the constraints on the model parameters from the global EW fit in view of the latest CDF m_W measurement, and then investigate the possibility of simultaneously explaining the observed W-boson mass shift and the $b \to s\ell^+\ell^-$ anomalies. Our conclusion is finally made in section 6. Details on the $b \to s\ell^+\ell^-$ fit are given in the appendix.

2. Model

As mentioned in the last section, to simultaneously accommodate the latest CDF W-boson mass shift and the $b \to s\ell^+\ell^-$ anomalies, the new fermions contributing to the vacuum polarization of gauge bosons should have the same quantum numbers as of the SM quarks. To this end, one simple realization is the Z' model introduced in ref. [51]. The model is characterized by a new $U(1)'$ gauge symmetry that is spontaneously broken by the vacuum expectation value (vev) of a new scalar field Φ, transforming as $(1, 1, 0, q_t)$ under the $SU(3)_C \otimes SU(2)_L \otimes U(1)_Y \otimes U(1)'$ gauge symmetry. While all the SM fields do not carry $U(1)'$ charge, a coloured singlet vector-like top partner $U'_{L,R}$, transforming as $(3, 1, 2/3, q_t)$, is introduced in the model. Specific to the case where only the third-generation SM quarks mix with the top partner, the general renormalizable interactions take the form [51,57]

$$\begin{aligned}\mathcal{L}_{\rm int} =& \left(\lambda_H \bar{Q}_{3L}\tilde{H}u_{3R} + \lambda_\Phi \bar{U}'_L u_{3R}\Phi + \mu \bar{U}'_L U'_R + \text{h.c.}\right) \\ &+ q_t g_t \left(\bar{U}'_L \gamma^\mu U'_L + \bar{U}'_R \gamma^\mu U'_R\right) Z'_\mu ,\end{aligned} \tag{2}$$

where q_t and g_t denote the charge and coupling of the $U(1)'$ gauge symmetry, respectively. $Q_{3L} = (u_{3L}, d_{3L})^T$ and u_{3R} denote the third-generation left-handed quark doublet and right-handed quark singlet in the SM, respectively. Matter fields in the above Lagrangian are all given in the interaction eigenbasis.[1] Mixing of T with the first two generations is also allowed, but suffers from severe experimental constraints as discussed in refs. [59,60]. Therefore, as in refs. [51,57], such mixing is assumed to be small compared to the mixing with the third generation and is neglected. Furthermore, this assumption can be considered as a consequence of a (approximate) $U(2)$ symmetry [61–63] or underlying strongly-interacting dynamics [51,61]. For simplicity, the scalar potential and the interaction between Z' and Φ are suppressed here.[2]

After the $U(1)'$ and the EW symmetry breaking, where the vevs of the two scalar fields are given respectively by $\langle\Phi\rangle = v_\Phi/\sqrt{2}$ and $\langle H\rangle = v_H/\sqrt{2} \simeq 174$ GeV, both the SM fermions and the top partner as well as the Z' boson obtain their masses. By diagonalizing the mass matrix, the physical top quarks (t_L, t_R) and its partners (T_L, T_R) can be expressed in terms of the fermion fields in eq. (2) through the following rotation matrices [57]:

$$\begin{pmatrix} t_L \\ T_L \end{pmatrix} = \begin{pmatrix} \cos\theta_L & -\sin\theta_L \\ \sin\theta_L & \cos\theta_L \end{pmatrix} \begin{pmatrix} u_{3L} \\ U'_L \end{pmatrix}, \tag{3}$$

$$\begin{pmatrix} t_R \\ T_R \end{pmatrix} = \begin{pmatrix} \cos\theta_R & -\sin\theta_R \\ \sin\theta_R & \cos\theta_R \end{pmatrix} \begin{pmatrix} u_{3R} \\ U'_R \end{pmatrix}, \tag{4}$$

where the mixing angles θ_L and θ_R parameterize the rotation matrices of the left- and right-handed quarks, respectively. In terms of the physical parameters, the top-quark mass m_t, the top-partner mass m_T, as well as the Z'-boson mass $m_{Z'} = g_t v_\Phi$, the two mixing angles are related to each other through

$$\tan\theta_L = \frac{m_t}{m_T}\tan\theta_R , \tag{5}$$

with m_t and m_T determined, respectively, by

$$\begin{aligned}\lambda_H &= \frac{\cos\theta_L}{\cos\theta_R}\frac{\sqrt{2}m_t}{v_H}, \\ |\lambda_\Phi| &= g_t\,|\cos\theta_L \sin\theta_R|\,\frac{\sqrt{2}m_T}{m_{Z'}}\left(1 - \frac{m_t^2}{m_T^2}\right).\end{aligned} \tag{6}$$

Turning to the fermion mass eigenbasis, the explicit expressions of the gauge interactions involving the top quark and the top partner can be written as [51,57]

$$\mathcal{L}_\gamma = \frac{2}{3}e\bar{t}\not{A}t + \frac{2}{3}e\bar{T}\not{A}T , \tag{7}$$

$$\mathcal{L}_W = \frac{g}{\sqrt{2}}V_{td_i}\left(c_L\bar{t}\not{W}P_L d_i + s_L\bar{T}\not{W}P_L d_i\right) + \text{ h.c.}, \tag{8}$$

$$\begin{aligned}\mathcal{L}_Z =& \frac{g}{c_W}\left(\bar{t}_L, \bar{T}_L\right)\begin{pmatrix} \frac{1}{2}c_L^2 - \frac{2}{3}s_W^2 & \frac{1}{2}s_L c_L \\ \frac{1}{2}s_L c_L & \frac{1}{2}s_L^2 - \frac{2}{3}s_W^2 \end{pmatrix}\not{Z}\begin{pmatrix} t_L \\ T_L \end{pmatrix} \\ &+ \frac{g}{c_W}\left(\bar{t}_R, \bar{T}_R\right)\left(-\frac{2}{3}s_W^2\right)\not{Z}\begin{pmatrix} t_R \\ T_R \end{pmatrix},\end{aligned} \tag{9}$$

$$\begin{aligned}\mathcal{L}_{Z'} =& q_t g_t \left(\bar{t}_L, \bar{T}_L\right)\begin{pmatrix} s_L^2 & -s_L c_L \\ -s_L c_L & c_L^2 \end{pmatrix}\not{Z}'\begin{pmatrix} t_L \\ T_L \end{pmatrix} \\ &+ (L \to R),\end{aligned} \tag{10}$$

where $s_{L,R} = \sin\theta_{L,R}$, $c_{L,R} = \cos\theta_{L,R}$, and $s_W = \sin\theta_W$ with the Weinberg mixing angle θ_W; d_i stand for the down-type quarks d, s, b, g denotes the SM weak coupling constant, and V_{td_i} are the CKM matrix elements. In eq. (8), V_{td_i} arise from the rotation among the left-handed down-type quarks, while c_L and s_L from the rotation in eq. (3). The Yukawa interactions of the physical SM Higgs h with the top quark and the top partner are given by

$$\mathcal{L}_h = -\frac{m_t}{v_H}c_L\left(\bar{t}_L, \bar{T}_L\right)\begin{pmatrix} c_L & c_L\tan\theta_R \\ s_L & s_L\tan\theta_R \end{pmatrix} h \begin{pmatrix} t_R \\ T_R \end{pmatrix} + \text{h.c.} \tag{11}$$

The quark sector of this model is similar to the generic vector-like quark models, which have been extensively studied in the literature [59,60,64–72].

Assuming that the effective Z' couplings to the charged leptons are flavour diagonal and focusing only on its interaction with the muon, we can then write the general renormalizable $\mu^+\mu^- Z'$ vertex as [51,57,73]

$$\mathcal{L}_\mu = \bar{\mu}\not{Z}'\left(g_\mu^L P_L + g_\mu^R P_R\right)\mu , \tag{12}$$

where the effective couplings g_μ^L and g_μ^R depend on the specific UV completions. Generally, extra chiral or vector-like fermions should also be added to make the UV models anomaly-free. For example, vector-like leptonic partners are introduced in ref. [74]. In this letter, since we only concentrate on the possible connection

[1] We choose the basis where the up-type Yukawa matrix is diagonal in the SM flavour space. In this basis, the first two generations coincide with their mass eigenstates. Thus, when diagonalizing the mass matrix, only the rotation between u_3 and U' is needed in the up sector, and the CKM is defined by the rotation among down-type quarks. See refs. [59,60] for more details.

[2] Generally, the potential contains the term $\lambda H^\dagger H|\Phi|^2$, which induces the mixing between the Higgs and the scalar Φ. Thus, the Higgs couplings are universally reduced and the oblique parameters should also be affected. In this work, as in ref. [51], the coupling λ is assumed to be small so that these effects can be neglected.

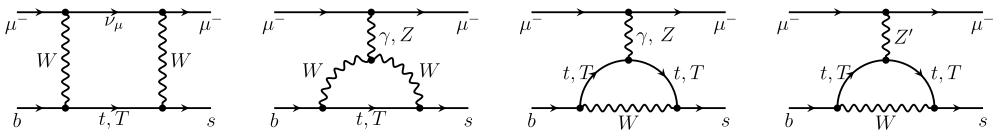

Fig. 1. One-loop Feynman diagrams for the $b \to s\mu^+\mu^-$ transitions, corresponding to the W-box, as well as the γ-, Z-, and Z'-penguin contributions, respectively.

between the latest CDF W-boson mass shift and the $b \to s\mu^+\mu^-$ anomalies, details of the lepton sector are not so much relevant. Thus, as in refs. [51,57,73], we shall consider the general effective $\mu^+\mu^- Z'$ interaction and leave the complete UV completions for future work.

3. W-boson mass shift and oblique parameters

The global fit of the SM to the EW precision data, known as the global EW fit [8–10], is a powerful tool to explore the validity of the SM and provides also a sensitive probe of NP beyond it [75–78]. As the EW parameters of the SM are closely related to each other, it is generally expected that some observables in the global EW fit may be affected once the latest CDF m_W measurement is considered [13–17]. Most of the NP effects on the EW sector can be parameterized in terms of the oblique parameters S, T and U [79–81]. These parameters are in turn related to the NP contributions to the vacuum polarization of gauge bosons and can be written, respectively, as [79,80]

$$S = \frac{4s_W^2 c_W^2}{\alpha}\left[\frac{\Pi_{ZZ}\left(m_Z^2\right) - \Pi_{ZZ}(0)}{m_Z^2} - \frac{c_W^2 - s_W^2}{s_W c_W}\Pi'_{Z\gamma}(0) - \Pi'_{\gamma\gamma}(0)\right], \tag{13}$$

$$T = \frac{1}{\alpha}\left[\frac{\Pi_{WW}(0)}{m_W^2} - \frac{\Pi_{ZZ}(0)}{m_Z^2}\right], \tag{14}$$

$$U = \frac{4s_W^2}{\alpha}\left[\frac{\Pi_{WW}\left(m_W^2\right) - \Pi_{WW}(0)}{m_W^2} - \frac{c_W}{s_W}\Pi'_{Z\gamma}(0) - \Pi'_{\gamma\gamma}(0)\right] - S\,, \tag{15}$$

where Π_{XY} denotes the NP contribution to the vacuum polarization of the gauge bosons with $X, Y = W, Z, \gamma$, $c_W = \cos\theta_W$, and α is the fine structure constant. Then, the W-boson mass shift induced by the oblique corrections can be expressed as [79]

$$\Delta m_W^2 = \frac{\alpha c_W^2 m_Z^2}{c_W^2 - s_W^2}\left[-\frac{S}{2} + c_W^2 T + \frac{c_W^2 - s_W^2}{4s_W^2}U\right]. \tag{16}$$

Thus, to make an explanation of the discrepancy between the latest CDF m_W measurement and the SM expectation, one needs a global EW fit to the oblique parameters S, T and U, which encode the potential NP effects.

In the model introduced in section 2, extra contributions to the vacuum polarization of gauge bosons arise from the modified fermion-gauge couplings that are characterized by the mixing angle θ_L, as well as from the loops involving the top partner (cf. eqs. (7)–(10)). Their contributions to the oblique parameters can be written as

$$S = \frac{s_L^2}{12\pi}\left[K_1(y_t, y_T) + 3c_L^2 K_2(y_t, y_T)\right], \tag{17}$$

$$T = \frac{3s_L^2}{16\pi s_W^2}\left[x_T - x_t - c_L^2\left(x_T + x_t + \frac{2x_t x_T}{x_T - x_t}\ln\frac{x_t}{x_T}\right)\right], \tag{18}$$

$$U = \frac{s_L^2}{12\pi}\left[K_3(x_t, y_t) - K_3(x_T, y_T)\right] - S, \tag{19}$$

with $x_q = m_q^2/m_W^2$ and $y_q = m_q^2/m_Z^2$ for $q = t, T$. Explicit expressions of the loop functions $K_{1,2,3}(x, y)$ are listed in the supplementary material. These results have been calculated in ref. [67] in a more general case. In the NP model considered, the oblique parameters S, T and U are solely determined by the two NP parameters θ_L and m_T.

In addition, $Z - Z'$ mixing, which arise from the top (top partner) loops, could also affect the EW observables. In the model considered, we find that the leading contribution results in the mixing term $\mathcal{L}_{\rm mix} = \delta m^2 Z'_\mu Z^\mu$ with

$$\delta m^2 = \frac{3eq_t g_t s_L^2}{32\pi^2 s_W c_W}\left(c_L^2 I_L + c_R^2 I_R\right), \tag{20}$$

where $I_{L,R}$ depend on m_t and m_T and are given in the supplementary material. Such a mixing term should contribute to the $Z \to \mu^+\mu^-$ decay, as in the EFT analysis in ref. [82]. Thus, strong bounds on the products $q_t g_t g_{L,R}$ are expected. However, as mentioned in section 2, the lepton sector in a UV-complete model should contain other NP particles, which may also affect the $Z \to \mu^+\mu^-$ decay. As a consequence, the bounds in a UV-complete model could be different from the ones in the framework with an effective $Z\mu^+\mu^-$ coupling. The former could be weaker or stronger than the latter, depending on interference between the different NP contributions. Thus, to be conservative, bounds from the $Z - Z'$ mixing will be derived in our numerical analysis, but they will not be combined with other constraints.

4. $b \to s\ell^+\ell^-$ transitions

The FCNC processes mediated by the quark-level $b \to s\ell^+\ell^-$ transitions, such as the rare decays $B_s \to \ell^+\ell^-$, $B \to K^{(*)}\ell^+\ell^-$ and $B_s \to \phi\ell^+\ell^-$, can also provide promising probes of potential NP effects [5–7]. Specific to the model introduced in section 2, the NP contributions to the $b \to s\ell^+\ell^-$ transitions start at the one-loop level, with the relevant Feynman diagrams shown in Fig. 1. Here the NP effects can arise from the modified SM box and penguin diagrams that are featured by the mixing angle θ_L, as well as from the penguin diagrams involving the top partner and/or Z' boson.

By an explicit calculation, we find that these NP contributions affect only the Wilson coefficients $\mathcal{C}_9$ and $\mathcal{C}_{10}$ in the low-energy effective weak Hamiltonian governing the $b \to s\mu^+\mu^-$ transitions [83]

$$\mathcal{H}_{\rm eff} \supset -\frac{4G_F}{\sqrt{2}}V_{tb}V_{ts}^*\frac{\alpha}{4\pi}\left(\mathcal{C}_9^\mu\mathcal{O}_9^\mu + \mathcal{C}_{10}^\mu\mathcal{O}_{10}^\mu\right) + \text{h.c.}\,, \tag{21}$$

with the four-fermion operators $\mathcal{O}_9 = \left(\bar{s}\gamma^\mu P_L b\right)\left(\bar{\mu}\gamma_\mu\mu\right)$ and $\mathcal{O}_{10} = \left(\bar{s}\gamma^\mu P_L b\right)\left(\bar{\mu}\gamma_\mu\gamma_5\mu\right)$. Explicitly, the NP contributions to $\mathcal{C}_9$ and $\mathcal{C}_{10}$ can be written, respectively, as

$$\mathcal{C}_9^{\rm NP} = s_L^2 I_1 + s_L^2\left(1 - \frac{1}{4s_W^2}\right)\left(I_2 + c_L^2 I_3\right) + \Delta\mathcal{C}_+^{Z'}\,, \tag{22}$$

$$\mathcal{C}_{10}^{\rm NP} = \frac{s_L^2}{4s_W^2}\left(I_2 + c_L^2 I_3\right) + \Delta\mathcal{C}_-^{Z'}\,, \tag{23}$$

with the Z'-penguin contributions given by

$$\Delta C_{\pm}^{Z'} = \frac{(g_R \pm g_L) q_t g_t}{e^2} \frac{m_W^2}{m_{Z'}^2} c_L^2 s_R^2 \left(I_4 - \frac{c_L^2}{c_R^2} I_5 \right), \tag{24}$$

where $e = \sqrt{4\pi\alpha}$ is the electromagnetic coupling constant. The loop integrals I_{1-5} are all functions of the masses m_t and m_T, whose explicit expressions can be found in the supplementary material. In the limit of $\theta_L \to 0$ or $\theta_R \to 0$, the NP Wilson coefficients $\mathcal{C}_9^{\rm NP}$ and $\mathcal{C}_{10}^{\rm NP}$ will vanish.

Here, the NP contributions to the Wilson coefficients $\mathcal{C}_9^{\rm NP}$ and $\mathcal{C}_{10}^{\rm NP}$ are calculated in the unitary gauge. We implement our computation in two setups by making use of different packages including `FeynRules` [84], `FeynArts` [85], `FeynCalc` [86–88], `Package-X` [89], as well as some in-house routines. After expanding in terms of the ratio m_W^2/m_T^2 and keeping only the leading terms in $s_R = \sin\theta_R$, our results are in agreement with those obtained in ref. [57].

5. Numerical analysis

5.1. W-boson mass and global EW fit

As all the three oblique parameters S, T and U could be affected by the NP effects (cf. eqs. (17)–(19)), a global EW fit is required to explain the latest CDF m_W measurement [11]. To this end, several groups have recently updated the global EW fit on the S, T and U parameters by including the latest CDF measurement of the W-bosn mass [13–17]. Here, we adopt the result obtained in ref. [16],[3] which is based on the package `Gfitter` [75–77]. The resulting values of the S, T and U parameters as well as the correlation matrix read [16]

$$\begin{aligned} &S = 0.06 \pm 0.10, \\ &T = 0.11 \pm 0.12, \\ &U = 0.14 \pm 0.09, \end{aligned} \quad \text{corr.} = \begin{bmatrix} 1.00 & 0.90 & -0.59 \\ & 1.00 & -0.85 \\ & & 1.00 \end{bmatrix}. \tag{25}$$

As described in section 3, the NP contributions to the S, T and U parameters depend only on the top-partner mass m_T and the mixing angle θ_L. To avoid large modification of the $\bar{t}bW^+$ coupling, we require $\cos\theta_L > 0.9$ in the following. This range is also consistent with that derived from the top-Higgs coupling through global fits to the SM Higgs properties [52,57]. After considering the constraints from the global EW fit, we find that there still exist parameter regions allowed at 2σ level, which is shown in Fig. 2. Numerically, $\cos\theta_L = 0.98 \sim 0.99$ is allowed for $500 < m_T < 2000$ GeV. For comparison, results by considering the EW fit with the average for m_W which includes the CDF result together with the previous measurements [17] have been also shown in Fig. 2, where the allowed $\cos\theta_L$ values become larger. In supplementary material, predictions on S, T and U from the allowed regions in Fig. 2 are also given.

Such a small mixing angle suppresses the NP contributions from the W-box, γ- and Z-penguin diagrams, because they are all proportional to $\sin^2\theta_L$, as can be seen from eqs. (22) and (23). However, the Z'-penguin diagrams do not suffer from this suppression and may affect the $b \to s\ell^+\ell^-$ processes, as will be exploited in the next subsection.

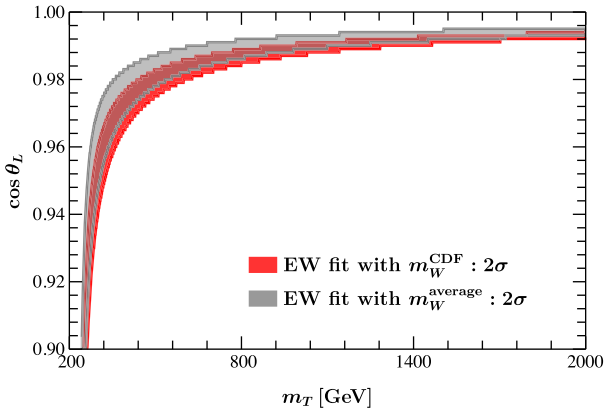

Fig. 2. Allowed parameter space in the $(m_T, \cos\theta_L)$ plane at 2σ level from the global EW fit with the latest CDF measurement of the W-boson mass. Result by considering the m_W average which includes the CDF result together with the previous measurements is also shown in the dark region.

5.2. $b \to s\ell^+\ell^-$ anomalies

In the model considered, the NP affects only the Wilson coefficients $\mathcal{C}_9$ and $\mathcal{C}_{10}$ and, in order to find the parameter regions required to explain the $b \to s\ell^+\ell^-$ anomalies, we perform a global fit to $b \to s\ell^+\ell^-$ data. Details of the fit are described in the appendix.

The NP contributions to the $b \to s\ell^+\ell^-$ transitions depend on the mixing angles $\theta_{L,R}$, the top-partner mass m_T, the $U(1)'$ charge q_t, the Z' mass $m_{Z'}$, the $\bar{t}tZ'$ coupling g_t, as well as the $\mu^+\mu^-Z'$ couplings $g_\mu^{L,R}$. From eqs. (22) and (23), one can see that the Z'-related parameters always appear as the product $q_t g_t g_\mu^{L,R}/m_{Z'}^2$. Thus, without loss of generality, we take in the numerical analysis $q_t = 1$, $g_t = 1$ and $m_{Z'} = 200$ GeV, while keeping the effective $\mu^+\mu^-Z'$ couplings $g_\mu^{L,R}$ as free parameters. After considering the relation in eq. (5), the independent NP parameters can be chosen as $(\cos\theta_L, m_T, g_\mu^L, g_\mu^R)$.

With the 2σ allowed regions of $\cos\theta_L$ and m_T obtained from the global EW fit (cf. Fig. 2), constraints on the NP parameters $g_\mu^{L,R}$ can then be derived from the $b \to s\ell^+\ell^-$ processes. In Fig. 3, we show the allowed regions of (g_μ^L, g_μ^R) for $m_T = 500$, 1000, 1500, 2000 GeV, respectively. It can be seen that, even after considering the latest CDF measurement of the W-boson mass, the model introduced in section 2 can still accommodate the $b \to s\ell^+\ell^-$ anomalies. For a Z' boson with mass of hundreds of GeV, its couplings to the top and the muon are both less than $\mathcal{O}(1)$, being therefore safely in the perturbative region. Taking $q_t = 1$ and considering the perturbativity bound $g_{t,L,R} \leq 4\pi$, upper bounds on the Z' mass can be obtained as $m_{Z'} \leq 7.0$, 12.7, 17.2, 20.9 TeV for $m_T = 0.5$, 1.0, 1.5, 2.0 TeV, respectively. In Fig. 3, ranges of the ratio g_R/g_L are almost the same for different m_T and are found to be $-0.4 < g_R/g_L < 0.7$ in the 2σ allowed region, which corresponds to $-7 < \mathcal{C}_9^{\rm NP}/\mathcal{C}_{10}^{\rm NP} < -0.4$ (-6.3 for the best-fit point).[4] Furthermore, the allowed regions shrink dramatically as m_T is increased. The reason is that, for heavier top partner, the Wilson coefficients $\mathcal{C}_{9,10}^{\rm NP}$ are enhanced by larger $\cos\theta_L$ and $\sin\theta_R$ (cf. Fig. 2 and eq. (5)) as well as the $(m_T/m_W)^2$ terms (cf. eq. (24)).

[3] It is found that using the global EW fit performed in ref. [17] with the package `HEPfit` [90] does not make substantial changes to our numerical results.

[4] Recently, CMS announced their measurements $\bar{\mathcal{B}}(B_s \to \mu^+\mu^-) = (3.83^{+0.38+0.19+0.14}_{-0.36-0.16-0.13}) \times 10^{-9}$ corresponding to an integrated luminosity of 140 fb^{-1} [91]. After including it, the world average becomes more consistent with the SM prediction, thus making the $b \to s\ell^+\ell^-$ fit favour the case of $\mathcal{C}_9^{\rm NP} \gg \mathcal{C}_{10}^{\rm NP}$ or single $\mathcal{C}_9^{\rm NP}$ [92].

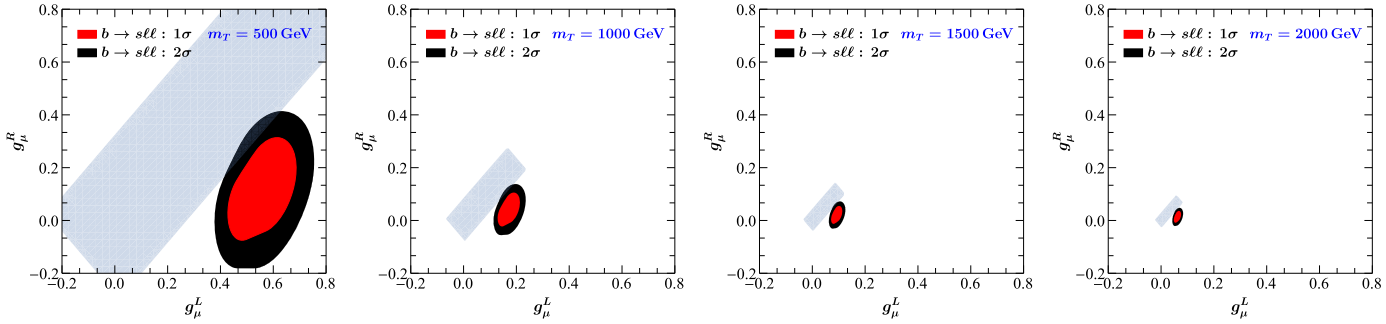

Fig. 3. Constraints on the effective $\mu^+\mu^- Z'$ couplings (g_μ^L, g_μ^R) by the $b \to s\ell^+\ell^-$ processes, in the 2σ allowed regions of the $(\cos\theta_L, m_T)$ plane obtained from the global EW fit with the latest CDF m_W measurement. The allowed regions are shown in red (1σ) and black (2σ) for $m_T = 500$, 1000, 1500, 2000 GeV, respectively. Here, without loss of generality, $q_t = 1$, $g_t = 1$ and $m_{Z'} = 200$ GeV have been taken. For comparison, constraints from the $Z \to \mu^+\mu^-$ decay induced by the $Z - Z'$ mixing are also shown in the dark region.

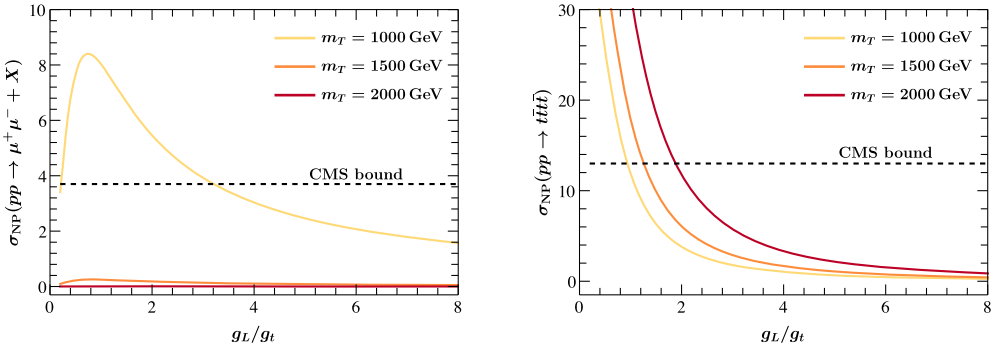

Fig. 4. NP contributions to the cross sections of $pp \to \mu^+\mu^- + X$ (left) and $pp \to t\bar{t}t\bar{t}$ (right), and 95% C.L. upper bounds from the CMS experiment [93,94]. The lines correspond to the benchmark points (See text for more details.) at $m_T = 1000$, 1500 and 2000 GeV.

We also derive the constraints from the $Z \to \mu^+\mu^-$ decay in the presence of the $Z - Z'$ mixing, as in ref. [82], which are shown in Fig. 3. However, as mentioned in section 2, such constraints could be quite different in a UV-complete model for the lepton sector. Thus, they are not combined with the constraints from the $b \to s\ell^+\ell^-$ fit.

5.3. Collider searches

Direct searches for single and pair productions of the vector-like top partner have been performed at the LHC, and strong bounds on the mass and mixing angle of the top partner have been derived [71,95–97]. However, most of these searches assume that the top partner decays exclusively into the SM particles, *i.e.*, $T \to bW/tZ/th$. Then, m_T below 1.3 TeV is excluded, which applies for the case of $m_{Z'} > m_T$. However, in the range $m_{Z'} < m_T - m_t$, $T \to tZ'$ channel is open and could relax the constraints from these direct searches [98–100].

In the model considered, the Z' boson couples exclusively to the top quark and the top partner. Collider phenomenologies of such a top-philic Z' have been investigated in refs. [51,54–57]. The $Z' \to \mu^+\mu^-$ decay makes the dimuon resonance searches [94,101] sensitive to this scenario. In addition, searches for multi-top final states [93,102] could also provide important constraints [57]. In order to estimate the collider constraints, we fix $m_{Z'} = 500$ GeV, $m_\Phi = 150$ GeV, $q_t = 1$, and $g_R = 0$. In the allowed regions in Fig. 2 and Fig. 3, three benchmark points are chosen with $(m_T, \sin\theta_L, g_L g_t) = (1.0\text{ TeV}, 0.988, 0.72)$, $(1.5\text{ TeV}, 0.993, 0.54)$, and $(2.0\text{ TeV}, 0.994, 0.35)$. For the dimuon resonance search, the cross section is estimated by $\sigma(pp \to T\bar{T}) \cdot 2 \cdot \mathcal{B}(T \to tZ') \cdot \mathcal{B}(Z' \to \mu^+\mu^-)$. Predictions for each benchmark point are shown as a function of g_L/g_t in Fig. 4. In this figure, we also show the NP contributions to $\sigma(pp \to t\bar{t}t\bar{t})$, which is estimated by $\sigma(pp \to t\bar{t}Z') \cdot \mathcal{B}(Z' \to t\bar{t})$. It can be seen that the collider constraints yield lower bounds on the ratio g_L/g_t, whose values are 1.5-3.2 depending on m_T. Different from the effective $Z'\mu^+\mu^-$ coupling, as mentioned in section 2, Z' boson could couple to τ, ν and NP particles in a UV-complete model. Thus, $\mathcal{B}(Z' \to \mu^+\mu^-)$ could be suppressed and the above collider bounds can be relaxed. A complete analysis of the collider searches may provide interesting constraints, which is the focus of our future work. See supplementary material for the relevant formulae used in the above analysis.

6. Conclusion

The latest CDF measurement of the W-boson mass shows about 7σ deviation from the SM expectation obtained by a global EW fit. We have pointed out that the latest CDF m_W measurement and the $b \to s\ell^+\ell^-$ anomalies could be simultaneously accommodated by introducing additional fermions, which have the same quantum numbers as of the SM quarks. As a simple example, the model introduced in ref. [51], which is characterized by a vector-like top partner with an additional $U(1)'$ gauge symmetry, is considered. We have calculated its contributions to the oblique parameters S, T and U in the global EW fit as well as the Wilson coefficients $\mathcal{C}_9$ and $\mathcal{C}_{10}$ in the $b \to s\ell^+\ell^-$ transitions. Our numerical results show that the top-partner loops in the vacuum polarization of gauge bosons can explain the latest CDF m_W measurement and, at the same time, the Z'-penguin diagrams involving the top partner can account for the $b \to s\ell^+\ell^-$ anomalies. Both the Z' boson and the top partner can be as light as of a few hundreds of GeV and thus may be accessible at the LHC Run III and its upgrade. Therefore, our work has demonstrated that the latest CDF W-boson mass shift could be related to the $b \to s\ell^+\ell^-$ anomalies, which is expected to inspire more complete model buildings for unified theories containing new fermions.

7. Note added

As this letter was being finalized, refs. [40–45,103] appeared that also consider possible explanations of the latest CDF m_W measurement with vector-like top partners.

Declaration of competing interest

The authors declare that they have no known competing financial interests or personal relationships that could have appeared to influence the work reported in this paper.

Data availability

Data will be made available on request.

Acknowledgements

This work is supported by the National Natural Science Foundation of China under Grant Nos. 12135006, 12075097, and 11805077, as well as by the self-determined research funds of CCNU from the colleges' basic research and operation of MOE under Grant Nos. CCNU19TD012, CCNU20TS007 and CCNU22LJ004. XY is also supported in part by the Startup Research Funding from CCNU.

Appendix A. $b \to s\ell^+\ell^-$ global fit

In the $b \to s\ell^+\ell^-$ global fit, as in refs. [92,104–106], we consider the following experimental data: 1) branching ratios of the decays $B \to K\mu^+\mu^-$ [107], $B \to K^*\mu^+\mu^-$ [107–110], $B_s \to \phi\mu^+\mu^-$ [111], $\Lambda_b \to \Lambda\mu^+\mu^-$ [112], $B \to X_s\mu^+\mu^-$ [113], and $B_s \to \mu^+\mu^-$ [114]. 2) angular distributions in $B \to K\mu^+\mu^-$ [108,115], $B \to K^*\mu^+\mu^-$ [49,50,109,116–118], $B_s \to \phi\mu^+\mu^-$ [119], and $\Lambda_b \to \Lambda\mu^+\mu^-$ [120] decays. 3) LFU ratios $R_{K^{(*)}}$ [46–48,121–125]. See supplementary material for their experimental values in each q^2 bin.

In the fit, following the approach in ref. [126], we construct a likelihood function that only depends on the Wilson coefficients as

$$-2\log L(\mathcal{C}) = \boldsymbol{x}^T(\mathcal{C})\big[V_{\rm exp} + V_{\rm th}(\boldsymbol{\theta})\big]^{-1}\boldsymbol{x}(\mathcal{C}),$$

with $\boldsymbol{x}_i(\mathcal{C}) = \mathcal{O}_i^{\rm exp} - \mathcal{O}_i^{\rm th}(\mathcal{C},\boldsymbol{\theta})$. Here, $\mathcal{O}_i^{\rm exp}$ and $\mathcal{O}_i^{\rm th}$ denote the central values of the experimental measurements and the theoretical predictions, respectively. They depend on the Wilson coefficients $\mathcal{C}$ and the input parameters $\boldsymbol{\theta}$. $V_{\rm exp}$ is the covariance matrix of the experimental measurements, while $V_{\rm th}$ denotes the covariance matrix of the theoretical predictions, which contains all the theoretical uncertainties and their correlations. Approximately, $V_{\rm th}$ is evaluated with the Wilson coefficients $\mathcal{C}$ fixed to their SM values. Furthermore, the theoretical uncertainties are approximated as Gaussian and obtained by randomly sampling the observables with the input parameters $\boldsymbol{\theta}$ distributed according to their probability density functions. Finally, the $\Delta\chi^2$ function can be written as $\Delta\chi^2(\mathcal{C}) = -2\log L(\mathcal{C})/L_{\rm max}$, where $L_{\rm max}$ denotes the maximum of L at different values of the Wilson coefficients. We refer to refs. [126–128], for more details on the fit methodology. Our global fit is performed by using an extended version of the package `flavio` [127]. See refs. [92,129–132] for the latest global fits by other groups, as well as ref. [133] for the fit by the package `smelli` [134].

Appendix B. Supplementary material

Supplementary material related to this article can be found online at https://doi.org/10.1016/j.physletb.2022.137651.

References

[1] P. Zyla, et al., Review of particle physics, Prog. Theor. Exp. Phys. 2020 (8) (2020) 083C01, https://doi.org/10.1093/ptep/ptaa104, and 2021 update.
[2] G. Aad, et al., Observation of a new particle in the search for the standard model Higgs boson with the ATLAS detector at the LHC, Phys. Lett. B 716 (2012) 1–29, https://doi.org/10.1016/j.physletb.2012.08.020, arXiv:1207.7214.
[3] S. Chatrchyan, et al., Observation of a new boson at a mass of 125 GeV with the CMS experiment at the LHC, Phys. Lett. B 716 (2012) 30–61, https://doi.org/10.1016/j.physletb.2012.08.021, arXiv:1207.7235.
[4] I. Zurbano Fernandez, et al., High-Luminosity Large Hadron Collider (HL-LHC), Technical design report 10/2020, 12 2020, https://doi.org/10.23731/CYRM-2020-0010.
[5] S. Bifani, S. Descotes-Genon, A. Romero Vidal, M.-H. Schune, Review of lepton universality tests in B decays, J. Phys. G 46 (2) (2019) 023001, https://doi.org/10.1088/1361-6471/aaf5de, arXiv:1809.06229.
[6] J. Albrecht, D. van Dyk, C. Langenbruch, Flavour anomalies in heavy quark decays, Prog. Part. Nucl. Phys. 120 (2021) 103885, https://doi.org/10.1016/j.ppnp.2021.103885, arXiv:2107.04822.
[7] D. London, J. Matias, B flavour anomalies: 2021 theoretical status report, 10 2021, arXiv:2110.13270, https://doi.org/10.1146/annurev-nucl-102020-090209.
[8] W.F.L. Hollik, Radiative corrections in the standard model and their role for precision tests of the electroweak theory, Fortschr. Phys. 38 (1990) 165–260, https://doi.org/10.1002/prop.2190380302.
[9] P. Langacker, M.-x. Luo, A.K. Mann, High precision electroweak experiments: a global search for new physics beyond the standard model, Rev. Mod. Phys. 64 (1992) 87–192, https://doi.org/10.1103/RevModPhys.64.87.
[10] J. Erler, M. Schott, Electroweak precision tests of the standard model after the discovery of the Higgs boson, Prog. Part. Nucl. Phys. 106 (2019) 68–119, https://doi.org/10.1016/j.ppnp.2019.02.007, arXiv:1902.05142.
[11] T. Aaltonen, et al., High-precision measurement of the W boson mass with the CDF II detector, Science 376 (6589) (2022) 170–176, https://doi.org/10.1126/science.abk1781.
[12] R. Aaij, et al., Measurement of the W boson mass, J. High Energy Phys. 01 (2022) 036, https://doi.org/10.1007/JHEP01(2022)036, arXiv:2109.01113.
[13] A. Strumia, Interpreting electroweak precision data including the W-mass CDF anomaly, 4 2022, arXiv:2204.04191.
[14] P. Asadi, C. Cesarotti, K. Fraser, S. Homiller, A. Parikh, Oblique lessons from the W mass measurement at CDF II, 4 2022, arXiv:2204.05283.
[15] J. Gu, Z. Liu, T. Ma, J. Shu, Speculations on the W-mass measurement at CDF, 4 2022, arXiv:2204.05296.
[16] C.-T. Lu, L. Wu, Y. Wu, B. Zhu, Electroweak precision fit and new physics in light of W boson mass, 4 2022, arXiv:2204.03796.
[17] J. de Blas, M. Pierini, L. Reina, L. Silvestrini, Impact of the recent measurements of the top-quark and W-boson masses on electroweak precision fits, 4 2022, arXiv:2204.04204.
[18] J. Fan, L. Li, T. Liu, K.-F. Lyu, W-boson mass, electroweak precision tests and SMEFT, 4 2022, arXiv:2204.04805.
[19] X. Liu, S.-Y. Guo, B. Zhu, Y. Li, Unifying gravitational waves with W boson, FIMP dark matter, and Majorana Seesaw mechanism, 4 2022, arXiv:2204.04834.
[20] E. Bagnaschi, J. Ellis, M. Madigan, K. Mimasu, V. Sanz, T. You, SMEFT analysis of m_W, 4 2022, arXiv:2204.05260.
[21] A. Paul, M. Valli, Violation of custodial symmetry from W-boson mass measurements, 4 2022, arXiv:2204.05267.
[22] Y. Heo, D.-W. Jung, J.S. Lee, Impact of the CDF W-mass anomaly on two Higgs doublet model, 4 2022, arXiv:2204.05728.
[23] M.-D. Zheng, F.-Z. Chen, H.-H. Zhang, The $W\ell\nu$-vertex corrections to W-boson mass in the R-parity violating MSSM, 4 2022, arXiv:2204.06541.
[24] E. d, S. Almeida, A. Alves, O.J.P. Eboli, M.C. Gonzalez-Garcia, Impact of CDF-II measurement of M_W on the electroweak legacy of the LHC Run I, 4 2022, arXiv:2204.10130.
[25] Y. Cheng, X.-G. He, F. Huang, J. Sun, Z.-P. Xing, Dark photon kinetic mixing effects for CDF W mass excess, 4 2022, arXiv:2204.10156.
[26] T.-K. Chen, C.-W. Chiang, K. Yagyu, Explanation of the W mass shift at CDF II in the Georgi-Machacek Model, 4 2022, arXiv:2204.12898.
[27] M. Algueró, A. Crivellin, C.A. Manzari, J. Matias, Importance of $Z - Z'$ mixing in $b \to s\ell^+\ell^-$ and the W mass, 1 2022, arXiv:2201.08170.
[28] Q. Zhou, X.-F. Han, The CDF W-mass, muon g-2, and dark matter in a $U(1)_{L_\mu - L_\tau}$ model with vector-like leptons, 4 2022, arXiv:2204.13027.
[29] O. Popov, R. Srivastava, The triplet Dirac seesaw in the view of the recent CDF-II W mass anomaly, 4 2022, arXiv:2204.08568.
[30] K. Ghorbani, P. Ghorbani, W-boson mass anomaly from scale invariant 2HDM, 4 2022, arXiv:2204.09001.
[31] A. Bhaskar, A.A. Madathil, T. Mandal, S. Mitra, Combined explanation of W-mass, muon $g-2$, $R_{K^{(*)}}$ and $R_{D^{(*)}}$ anomalies in a singlet-triplet scalar leptoquark model, 4 2022, arXiv:2204.09031.
[32] J.J. Heckman, Extra W-boson mass from a D3-brane, 4 2022, arXiv:2204.05302.

[33] L. Di Luzio, R. Gröber, P. Paradisi, Higgs physics confronts the M_W anomaly, 4 2022, arXiv:2204.05284.

[34] Y.-Z. Fan, T.-P. Tang, Y.-L.S. Tsai, L. Wu, Inert Higgs dark matter for new CDF W-boson mass and detection prospects, 4 2022, arXiv:2204.03693.

[35] T.-P. Tang, M. Abdughani, L. Feng, Y.-L.S. Tsai, Y.-Z. Fan, NMSSM neutralino dark matter for W-boson mass and muon $g-2$ and the promising prospect of direct detection, 4 2022, arXiv:2204.04356.

[36] D. Borah, S. Mahapatra, D. Nanda, N. Sahu, Type II Dirac seesaw with observable ΔN_{eff} in the light of W-mass anomaly, 4 2022, arXiv:2204.08266.

[37] K. Sakurai, F. Takahashi, W. Yin, Singlet extensions and W boson mass in the light of the CDF II result, 4 2022, arXiv:2204.04770.

[38] P. Athron, A. Fowlie, C.-T. Lu, L. Wu, Y. Wu, B. Zhu, The W boson mass and muon $g-2$: hadronic uncertainties or new physics?, 4 2022, arXiv:2204.03996.

[39] P. Athron, M. Bach, D.H.J. Jacob, W. Kotlarski, D. Stöckinger, A. Voigt, Precise calculation of the W boson pole mass beyond the standard model with FlexibleSUSY, 4 2022, arXiv:2204.05285.

[40] H.M. Lee, K. Yamashita, A model of vector-like leptons for the muon $g-2$ and the W boson mass, 4 2022, arXiv:2204.05024.

[41] A. Crivellin, M. Kirk, T. Kitahara, F. Mescia, Correlating $t \to cZ$ to the W mass and B physics with vector-like quarks, 4 2022, arXiv:2204.05962.

[42] M. Endo, S. Mishima, New physics interpretation of W-boson mass anomaly, 4 2022, arXiv:2204.05965.

[43] R. Balkin, E. Madge, T. Menzo, G. Perez, Y. Soreq, J. Zupan, On the implications of positive W mass shift, 4 2022, arXiv:2204.05992.

[44] J. Cao, L. Meng, L. Shang, S. Wang, B. Yang, Interpreting the W mass anomaly in the vectorlike quark models, 4 2022, arXiv:2204.09477.

[45] S. Baek, Implications of CDF W-mass and $(g-2)_\mu$ on $U(1)_{L_\mu - L_\tau}$ model, 4 2022, arXiv:2204.09585.

[46] R. Aaij, et al., Test of lepton universality with $B^0 \to K^{*0}\ell^+\ell^-$ decays, J. High Energy Phys. 08 (2017) 055, https://doi.org/10.1007/JHEP08(2017)055, arXiv:1705.05802.

[47] R. Aaij, et al., Test of lepton universality in beauty-quark decays, Nat. Phys. 18 (3) (2022) 277–282, https://doi.org/10.1038/s41567-021-01478-8, arXiv:2103.11769.

[48] R. Aaij, et al., Tests of lepton universality using $B^0 \to K^0_S\ell^+\ell^-$ and $B^+ \to K^{*+}\ell^+\ell^-$ decays, 10 2021, arXiv:2110.09501.

[49] R. Aaij, et al., Measurement of CP-averaged observables in the $B^0 \to K^{*0}\mu^+\mu^-$ decay, Phys. Rev. Lett. 125 (1) (2020) 011802, https://doi.org/10.1103/PhysRevLett.125.011802, arXiv:2003.04831.

[50] R. Aaij, et al., Angular analysis of the $B^+ \to K^{*+}\mu^+\mu^-$ decay, Phys. Rev. Lett. 126 (16) (2021) 161802, https://doi.org/10.1103/PhysRevLett.126.161802, arXiv:2012.13241.

[51] J.F. Kamenik, Y. Soreq, J. Zupan, Lepton flavor universality violation without new sources of quark flavor violation, Phys. Rev. D 97 (3) (2018) 035002, https://doi.org/10.1103/PhysRevD.97.035002, arXiv:1704.06005.

[52] P.J. Fox, J. Liu, D. Tucker-Smith, N. Weiner, An effective Z′, Phys. Rev. D 84 (2011) 115006, https://doi.org/10.1103/PhysRevD.84.115006, arXiv:1104.4127.

[53] J. Berger, J. Hubisz, M. Perelstein, A fermionic top partner: naturalness and the LHC, J. High Energy Phys. 07 (2012) 016, https://doi.org/10.1007/JHEP07(2012)016, arXiv:1205.0013.

[54] N. Greiner, K. Kong, J.-C. Park, S.C. Park, J.-C. Winter, Model-independent production of a top-philic resonance at the LHC, J. High Energy Phys. 04 (2015) 029, https://doi.org/10.1007/JHEP04(2015)029, arXiv:1410.6099.

[55] P. Cox, A.D. Medina, T.S. Ray, A. Spray, Novel collider and dark matter phenomenology of a top-philic Z', J. High Energy Phys. 06 (2016) 110, https://doi.org/10.1007/JHEP06(2016)110, arXiv:1512.00471.

[56] J.H. Kim, K. Kong, S.J. Lee, G. Mohlabeng, Probing TeV scale top-philic resonances with boosted top-tagging at the high luminosity LHC, Phys. Rev. D 94 (3) (2016) 035023, https://doi.org/10.1103/PhysRevD.94.035023, arXiv:1604.07421.

[57] P.J. Fox, I. Low, Y. Zhang, Top-philic Z' forces at the LHC, J. High Energy Phys. 03 (2018) 074, https://doi.org/10.1007/JHEP03(2018)074, arXiv:1801.03505.

[58] A. Crivellin, C.A. Manzari, M. Alguero, J. Matias, Combined explanation of the $Z \to b\bar{b}$ forward-backward asymmetry, the Cabibbo angle anomaly, $\tau \to \nu\nu$ and $b \to s\ell^+\ell^-$ data, Phys. Rev. Lett. 127 (1) (2021) 011801, https://doi.org/10.1103/PhysRevLett.127.011801, arXiv:2010.14504.

[59] S. Fajfer, A. Greljo, J.F. Kamenik, I. Mustac, Light Higgs and vector-like quarks without prejudice, J. High Energy Phys. 07 (2013) 155, https://doi.org/10.1007/JHEP07(2013)155, arXiv:1304.4219.

[60] J.A. Aguilar-Saavedra, Mixing with vector-like quarks: constraints and expectations, EPJ Web Conf. 60 (2013) 16012, https://doi.org/10.1051/epjconf/20136016012, arXiv:1306.4432.

[61] R. Barbieri, D. Buttazzo, F. Sala, D.M. Straub, Flavour physics from an approximate $U(2)^3$ symmetry, J. High Energy Phys. 07 (2012) 181, https://doi.org/10.1007/JHEP07(2012)181, arXiv:1203.4218.

[62] D.A. Faroughy, G. Isidori, F. Wilsch, K. Yamamoto, Flavour symmetries in the SMEFT, J. High Energy Phys. 08 (2020) 166, https://doi.org/10.1007/JHEP08(2020)166, arXiv:2005.05366.

[63] A. Greljo, A. Palavrić, A.E. Thomsen, Adding flavor to the SMEFT, 3 2022, arXiv:2203.09561.

[64] F. del Aguila, M.J. Bowick, The possibility of new fermions with Δ I = 0 mass, Nucl. Phys. B 224 (1983) 107, https://doi.org/10.1016/0550-3213(83)90316-4.

[65] G.C. Branco, L. Lavoura, On the addition of vector like quarks to the standard model, Nucl. Phys. B 278 (1986) 738–754, https://doi.org/10.1016/0550-3213(86)90060-X.

[66] P. Langacker, D. London, Mixing between ordinary and exotic fermions, Phys. Rev. D 38 (1988) 886, https://doi.org/10.1103/PhysRevD.38.886.

[67] L. Lavoura, J.P. Silva, The oblique corrections from vector - like singlet and doublet quarks, Phys. Rev. D 47 (1993) 2046–2057, https://doi.org/10.1103/PhysRevD.47.2046.

[68] F. del Aguila, M. Perez-Victoria, J. Santiago, Observable contributions of new exotic quarks to quark mixing, J. High Energy Phys. 09 (2000) 011, https://doi.org/10.1088/1126-6708/2000/09/011, arXiv:hep-ph/0007316.

[69] Y. Okada, L. Panizzi, LHC signatures of vector-like quarks, Adv. High Energy Phys. 2013 (2013) 364936, https://doi.org/10.1155/2013/364936, arXiv:1207.5607.

[70] S. Dawson, E. Furlan, A Higgs conundrum with vector fermions, Phys. Rev. D 86 (2012) 015021, https://doi.org/10.1103/PhysRevD.86.015021, arXiv:1205.4733.

[71] J.A. Aguilar-Saavedra, R. Benbrik, S. Heinemeyer, M. Pérez-Victoria, Handbook of vectorlike quarks: mixing and single production, Phys. Rev. D 88 (9) (2013) 094010, https://doi.org/10.1103/PhysRevD.88.094010, arXiv:1306.0572.

[72] S.A.R. Ellis, R.M. Godbole, S. Gopalakrishna, J.D. Wells, Survey of vector-like fermion extensions of the standard model and their phenomenological implications, J. High Energy Phys. 09 (2014) 130, https://doi.org/10.1007/JHEP09(2014)130, arXiv:1404.4398.

[73] A. Crivellin, L. Hofer, J. Matias, U. Nierste, S. Pokorski, J. Rosiek, Lepton-flavour violating B decays in generic Z' models, Phys. Rev. D 92 (5) (2015) 054013, https://doi.org/10.1103/PhysRevD.92.054013, arXiv:1504.07928.

[74] D. Aristizabal Sierra, F. Staub, A. Vicente, Shedding light on the $b \to s$ anomalies with a dark sector, Phys. Rev. D 92 (1) (2015) 015001, https://doi.org/10.1103/PhysRevD.92.015001, arXiv:1503.06077.

[75] H. Flacher, M. Goebel, J. Haller, A. Hocker, K. Monig, J. Stelzer, Revisiting the global electroweak fit of the standard model and beyond with Gfitter, Eur. Phys. J. C 60 (2009) 543–583, https://doi.org/10.1140/epjc/s10052-009-0966-6; Erratum: Eur. Phys. J. C 71 (2011) 1718, arXiv:0811.0009.

[76] M. Baak, J. Cúth, J. Haller, A. Hoecker, R. Kogler, K. Mönig, M. Schott, J. Stelzer, The global electroweak fit at NNLO and prospects for the LHC and ILC, Eur. Phys. J. C 74 (2014) 3046, https://doi.org/10.1140/epjc/s10052-014-3046-5, arXiv:1407.3792.

[77] J. Haller, A. Hoecker, R. Kogler, K. Mönig, T. Peiffer, J. Stelzer, Update of the global electroweak fit and constraints on two-Higgs-doublet models, Eur. Phys. J. C 78 (8) (2018) 675, https://doi.org/10.1140/epjc/s10052-018-6131-3, arXiv:1803.01853.

[78] J. de Blas, M. Ciuchini, E. Franco, A. Goncalves, S. Mishima, M. Pierini, L. Reina, L. Silvestrini, Global analysis of electroweak data in the standard mode, 12 2021, arXiv:2112.07274.

[79] M.E. Peskin, T. Takeuchi, Estimation of oblique electroweak corrections, Phys. Rev. D 46 (1992) 381–409, https://doi.org/10.1103/PhysRevD.46.381.

[80] M.E. Peskin, T. Takeuchi, A new constraint on a strongly interacting Higgs sector, Phys. Rev. Lett. 65 (1990) 964–967, https://doi.org/10.1103/PhysRevLett.65.964.

[81] I. Maksymyk, C.P. Burgess, Beyond S, T and U, Phys. Rev. D 50 (1994) 529–535, https://doi.org/10.1103/PhysRevD.50.529, arXiv:hep-ph/9306267.

[82] J.E. Camargo-Molina, A. Celis, D.A. Faroughy, Anomalies in bottom from new physics in top, Phys. Lett. B 784 (2018) 284–293, https://doi.org/10.1016/j.physletb.2018.07.051, arXiv:1805.04917.

[83] G. Buchalla, A.J. Buras, M.E. Lautenbacher, Weak decays beyond leading logarithms, Rev. Mod. Phys. 68 (1996) 1125–1144, https://doi.org/10.1103/RevModPhys.68.1125, arXiv:hep-ph/9512380.

[84] A. Alloul, N.D. Christensen, C. Degrande, C. Duhr, B. Fuks, FeynRules 2.0 - a complete toolbox for tree-level phenomenology, Comput. Phys. Commun. 185 (2014) 2250–2300, https://doi.org/10.1016/j.cpc.2014.04.012, arXiv:1310.1921.

[85] T. Hahn, Generating Feynman diagrams and amplitudes with FeynArts 3, Comput. Phys. Commun. 140 (2001) 418–431, https://doi.org/10.1016/S0010-4655(01)00290-9, arXiv:hep-ph/0012260.

[86] R. Mertig, M. Bohm, A. Denner, FEYN CALC: computer algebraic calculation of Feynman amplitudes, Comput. Phys. Commun. 64 (1991) 345–359, https://doi.org/10.1016/0010-4655(91)90130-D.

[87] V. Shtabovenko, R. Mertig, F. Orellana, New developments in FeynCalc 9.0, Comput. Phys. Commun. 207 (2016) 432–444, https://doi.org/10.1016/j.cpc.2016.06.008, arXiv:1601.01167.

[88] V. Shtabovenko, R. Mertig, F. Orellana, FeynCalc 9.3: new features and improvements, Comput. Phys. Commun. 256 (2020) 107478, https://doi.org/10.1016/j.cpc.2020.107478, arXiv:2001.04407.

[89] H.H. Patel, Package-X 2.0: a mathematica package for the analytic calculation of one-loop integrals, Comput. Phys. Commun. 218 (2017) 66–70, https://doi.org/10.1016/j.cpc.2017.04.015, arXiv:1612.00009.

[90] J. De Blas, et al., HEPfit: a code for the combination of indirect and direct constraints on high energy physics models, Eur. Phys. J. C 80 (5) (2020) 456, https://doi.org/10.1140/epjc/s10052-020-7904-z, arXiv:1910.14012.

[91] Measurement of $B_s^0 \to \mu^+\mu^-$ decay properties and search for the $B^0 \to \mu\mu$ decay in proton-proton collisions at $\sqrt{s} = 13$ TeV, 2022.

[92] W. Altmannshofer, P. Stangl, New physics in rare B decays after Moriond 2021, Eur. Phys. J. C 81 (10) (2021) 952, https://doi.org/10.1140/epjc/s10052-021-09725-1, arXiv:2103.13370.

[93] A.M. Sirunyan, et al., Search for production of four top quarks in final states with same-sign or multiple leptons in proton-proton collisions at $\sqrt{s} = 13$ TeV, Eur. Phys. J. C 80 (2) (2020) 75, https://doi.org/10.1140/epjc/s10052-019-7593-7, arXiv:1908.06463.

[94] A.M. Sirunyan, et al., Search for resonant and nonresonant new phenomena in high-mass dilepton final states at $\sqrt{s}$ = 13 TeV, J. High Energy Phys. 07 (2021) 208, https://doi.org/10.1007/JHEP07(2021)208, arXiv:2103.02708.

[95] M. Aaboud, et al., Combination of the searches for pair-produced vector-like partners of the third-generation quarks at $\sqrt{s} = 13$ TeV with the ATLAS detector, Phys. Rev. Lett. 121 (21) (2018) 211801, https://doi.org/10.1103/PhysRevLett.121.211801, arXiv:1808.02343.

[96] A. Tumasyan, et al., Search for single production of a vector-like T quark decaying to a top quark and a Z boson in the final state with jets and missing transverse momentum at $\sqrt{s}$ = 13 TeV, 1 2022, arXiv:2201.02227.

[97] H. de la TorreTrisha Farooque, T. Farooque, Looking beyond the standard model with third generation quarks at the LHC, Symmetry 14 (3) (2022) 444, https://doi.org/10.3390/sym14030444.

[98] J. Serra, Beyond the minimal top partner decay, J. High Energy Phys. 09 (2015) 176, https://doi.org/10.1007/JHEP09(2015)176, arXiv:1506.05110.

[99] A. Anandakrishnan, J.H. Collins, M. Farina, E. Kuflik, M. Perelstein, Odd top partners at the LHC, Phys. Rev. D 93 (7) (2016) 075009, https://doi.org/10.1103/PhysRevD.93.075009, arXiv:1506.05130.

[100] N. Bizot, G. Cacciapaglia, T. Flacke, Common exotic decays of top partners, J. High Energy Phys. 06 (2018) 065, https://doi.org/10.1007/JHEP06(2018)065, arXiv:1803.00021.

[101] G. Aad, et al., Search for high-mass dilepton resonances using 139 fb^{-1} of pp collision data collected at $\sqrt{s}$ =13 TeV with the ATLAS detector, Phys. Lett. B 796 (2019) 68–87, https://doi.org/10.1016/j.physletb.2019.07.016, arXiv:1903.06248.

[102] G. Aad, et al., Evidence for $t\bar{t}t\bar{t}$ production in the multilepton final state in proton–proton collisions at $\sqrt{s} = 13$ TeV with the ATLAS detector, Eur. Phys. J. C 80 (11) (2020) 1085, https://doi.org/10.1140/epjc/s10052-020-08509-3, arXiv:2007.14858.

[103] D. Borah, S. Mahapatra, N. Sahu, Singlet-doublet fermion origin of dark matter, neutrino mass and w-mass anomaly, 4 2022, arXiv:2204.09671.

[104] W. Altmannshofer, C. Niehoff, P. Stangl, D.M. Straub, Status of the $B \to K^*\mu^+\mu^-$ anomaly after Moriond 2017, Eur. Phys. J. C 77 (6) (2017) 377, https://doi.org/10.1140/epjc/s10052-017-4952-0, arXiv:1703.09189.

[105] W. Altmannshofer, P. Stangl, D.M. Straub, Interpreting hints for lepton flavor universality violation, Phys. Rev. D 96 (5) (2017) 055008, https://doi.org/10.1103/PhysRevD.96.055008, arXiv:1704.05435.

[106] J. Aebischer, W. Altmannshofer, D. Guadagnoli, M. Reboud, P. Stangl, D.M. Straub, B-decay discrepancies after Moriond 2019, Eur. Phys. J. C 80 (3) (2020) 252, https://doi.org/10.1140/epjc/s10052-020-7817-x, arXiv:1903.10434.

[107] R. Aaij, et al., Differential branching fractions and isospin asymmetries of $B \to K^{(*)}\mu^+\mu^-$ decays, J. High Energy Phys. 06 (2014) 133, https://doi.org/10.1007/JHEP06(2014)133, arXiv:1403.8044.

[108] CDF, Precise Measurements of Exclusive $b \to s\mu^+\mu^-$ Decay Amplitudes Using the Full CDF Data Set, 6 2012.

[109] V. Khachatryan, et al., Angular analysis of the decay $B^0 \to K^{*0}\mu^+\mu^-$ from pp collisions at $\sqrt{s} = 8$ TeV, Phys. Lett. B 753 (2016) 424–448, https://doi.org/10.1016/j.physletb.2015.12.020, arXiv:1507.08126.

[110] R. Aaij, et al., Measurements of the S-wave fraction in $B^0 \to K^+\pi^-\mu^+\mu^-$ decays and the $B^0 \to K^*(892)^0\mu^+\mu^-$ differential branching fraction, J. High Energy Phys. 11 (2016) 047, https://doi.org/10.1007/JHEP11(2016)047; Erratum: J. High Energy Phys. 04 (2017) 142, arXiv:1606.04731.

[111] R. Aaij, et al., Branching fraction measurements of the rare $B_s^0 \to \phi\mu^+\mu^-$ and $B_s^0 \to f_2'(1525)\mu^+\mu^-$ decays, 5 2021, arXiv:2105.14007.

[112] R. Aaij, et al., Differential branching fraction and angular analysis of $\Lambda_b^0 \to \Lambda\mu^+\mu^-$ decays, J. High Energy Phys. 06 (2015) 115, https://doi.org/10.1007/JHEP06(2015)115; Erratum: J. High Energy Phys. 09 (2018) 145, arXiv:1503.07138.

[113] J.P. Lees, et al., Measurement of the $B \to X_s l^+ l^-$ branching fraction and search for direct CP violation from a sum of exclusive final states, Phys. Rev. Lett. 112 (2014) 211802, https://doi.org/10.1103/PhysRevLett.112.211802, arXiv:1312.5364.

[114] R. Aaij, et al., Analysis of neutral B-meson decays into two muons, 8 2021, arXiv:2108.09284.

[115] R. Aaij, et al., Angular analysis of charged and neutral $B \to K\mu^+\mu^-$ decays, J. High Energy Phys. 05 (2014) 082, https://doi.org/10.1007/JHEP05(2014)082, arXiv:1403.8045.

[116] S. Wehle, et al., Lepton-flavor-dependent angular analysis of $B \to K^*\ell^+\ell^-$, Phys. Rev. Lett. 118 (11) (2017) 111801, https://doi.org/10.1103/PhysRevLett.118.111801, arXiv:1612.05014.

[117] CMS, Measurement of the P_1 and P_5' angular parameters of the decay $B^0 \to K^{*0}\mu^+\mu^-$ in proton-proton collisions at $\sqrt{s} = 8$ TeV, 2017.

[118] M. Aaboud, et al., Angular analysis of $B_d^0 \to K^*\mu^+\mu^-$ decays in pp collisions at $\sqrt{s} = 8$ TeV with the ATLAS detector, J. High Energy Phys. 10 (2018) 047, https://doi.org/10.1007/JHEP10(2018)047, arXiv:1805.04000.

[119] R. Aaij, et al., Angular analysis of the rare decay $B_s^0 \to \phi\mu^+\mu^-$, 7 2021, arXiv:2107.13428.

[120] R. Aaij, et al., Angular moments of the decay $\Lambda_b^0 \to \Lambda\mu^+\mu^-$ at low hadronic recoil, J. High Energy Phys. 09 (2018) 146, https://doi.org/10.1007/JHEP09(2018)146, arXiv:1808.00264.

[121] J.P. Lees, et al., Measurement of branching fractions and rate asymmetries in the rare decays $B \to K^{(*)}l^+l^-$, Phys. Rev. D 86 (2012) 032012, https://doi.org/10.1103/PhysRevD.86.032012, arXiv:1204.3933.

[122] A. Abdesselam, et al., Test of lepton flavor universality in $B \to K^*\ell^+\ell^-$ decays at Belle, arXiv:1904.02440, 2019.

[123] S. Choudhury, et al., Test of lepton flavor universality and search for lepton flavor violation in $B \to K\ell\ell$ decays, J. High Energy Phys. 03 (2021) 105, https://doi.org/10.1007/JHEP03(2021)105, arXiv:1908.01848.

[124] R. Aaij, et al., Search for lepton-universality violation in $B^+ \to K^+\ell^+\ell^-$ decays, Phys. Rev. Lett. 122 (19) (2019) 191801, https://doi.org/10.1103/PhysRevLett.122.191801, arXiv:1903.09252.

[125] R. Aaij, et al., Test of lepton universality in beauty-quark decays, 3 2021, arXiv:2103.11769.

[126] W. Altmannshofer, D.M. Straub, New physics in $b \to s$ transitions after LHC run 1, Eur. Phys. J. C 75 (8) (2015) 382, https://doi.org/10.1140/epjc/s10052-015-3602-7, arXiv:1411.3161.

[127] D.M. Straub, Flavio: a python package for flavour and precision phenomenology in the standard model and beyond, 10 2018, arXiv:1810.08132.

[128] X.-Q. Li, M. Shen, D.-Y. Wang, Y.-D. Yang, X.-B. Yuan, Explaining the $b \to s\ell^+\ell^-$ anomalies in Z' scenarios with top-FCNC couplings, 12 2021, arXiv:2112.14215.

[129] L.-S. Geng, B. Grinstein, S. Jäger, S.-Y. Li, J. Martin Camalich, R.-X. Shi, Implications of new evidence for lepton-universality violation in $b \to s\ell^+\ell^-$ decays, Phys. Rev. D 104 (3) (2021) 035029, https://doi.org/10.1103/PhysRevD.104.035029, arXiv:2103.12738.

[130] C. Cornella, D.A. Faroughy, J. Fuentes-Martin, G. Isidori, M. Neubert, Reading the footprints of the B-meson flavor anomalies, J. High Energy Phys. 08 (2021) 050, https://doi.org/10.1007/JHEP08(2021)050, arXiv:2103.16558.

[131] M. Algueró, B. Capdevila, S. Descotes-Genon, J. Matias, M. Novoa-Brunet, $b \to s\ell\ell$ global fits after R_{K_S} and $R_{K^{*+}}$, 4 2021, arXiv:2104.08921.

[132] T. Hurth, F. Mahmoudi, D.M. Santos, S. Neshatpour, More indications for lepton nonuniversality in $b \to s\ell^+\ell^-$, Phys. Lett. B 824 (2022) 136838, https://doi.org/10.1016/j.physletb.2021.136838, arXiv:2104.10058.

[133] B. Allanach, J. Davighi, M_W helps select Z' models for $b \to s\ell\ell$ anomalies, Eur. Phys. J. C 82 (8) (2022) 745, https://doi.org/10.1140/epjc/s10052-022-10693-3, arXiv:2205.12252.

[134] J. Aebischer, J. Kumar, P. Stangl, D.M. Straub, A global likelihood for precision constraints and flavour anomalies, Eur. Phys. J. C 79 (6) (2019) 509, https://doi.org/10.1140/epjc/s10052-019-6977-z, arXiv:1810.07698.